Published OnlineFirst January 18, 2018; DOI: 10.1158/1535-7163.MCT-17-0697

Large Molecule Therapeutics

Molecular Cancer Therapeutics

Intratumoral Payload Concentration Correlates with the Activity of Antibody–Drug Conjugates

Donglu Zhang[1], Shang-Fan Yu[2], S. Cyrus Khojasteh[1], Yong Ma[1], Thomas H. Pillow[3], Jack D. Sadowsky[4], Dian Su[1], Katherine R. Kozak[1], Keyang Xu[5], Andrew G. Polson[2], Peter S. Dragovich[3], and Cornelis E.C.A. Hop[1]

Abstract

Antibody–drug conjugates (ADC) have become important scaffolds for targeted cancer therapies. However, ADC exposure–response correlation is not well characterized. We demonstrated that intratumor payload exposures correlated well with the corresponding efficacies of several disulfide-linked ADCs, bearing an DNA alkylating agent, pyrrolo[2,1-c][1,4]benzodiazepine-dimer (PBD), in HER2-expressing xenograft models. The correlation suggests that a threshold concentration of intratumor payload is required to support sustained efficacy and an ADC can deliver an excessive level of payload to tumors that does not enhance efficacy ("Plateau" effect). In contrast to tumor PBD concentrations, related assessments of systemic exposures, plasma stability, and drug-to-antibody ratio changes of related ADCs did not consistently rationalize the observed ADC efficacies. A minimal efficacious dose could be determined by ADC dose-fractionation studies in the xenograft models. Mechanistic investigations revealed that both linker immolation and linker disulfide stability are the key factors that determine intratumor PBD concentrations. Overall, this study demonstrates how a linker design can impact ADC efficacy and that the intratumor exposure of a payload drug as the molecular mechanism quantitatively correlate with and predict the antitumor efficacy of ADCs. *Mol Cancer Ther; 17(3); 677–85.* ©*2018 AACR.*

Introduction

Antibody–drug conjugates (ADC) consist of an antibody that targets disease antigen(s) and a payload that is connected to the antibody via a linker. Such payloads are often potent antimitotic cytotoxins such as the maytansinoid present in ado-trastuzumab emtansine (Kadcyla, T-DM1) and the auristatin contained in brentuximab vedotin (Adcetris, MMAE; refs. 1, 2). More recently, potent DNA alkylating agents such as pyrrolo[2,1-c][1,4]benzodiazepine-dimers (PBD) have also been employed as ADC payloads (3, 4). An ADC can be viewed as a prodrug in which the circulating ADC as a reservoir slowly releases the active payload drug in tissues. The systemic pharmacokinetic (PK) profile of a typical ADC is mainly dictated by the antibody and is characterized by low clearance, small volume of distribution, long circulating half-life (days), and target or nontarget tissue distribution. Following internalization of an ADC, the payload is released into cells at a site of action to exert its biological activities (e.g., in tumor cells). The associated rate and extent of payload delivery is dependent on both tumor properties (such as antigen type, antigen expression and turnover rate, tumor type) and ADC characteristics including uptake, internalization, and biochemical transformation (proteolytic degradation of antibody, linker cleavage, and immolation to release payload). The levels of a given payload present at the site of action are determined by the amount of conjugate entering the tissue, the local ADC catabolism rate, and payload tissue-retention properties.

Although plasma concentration is in general a good surrogate for drug exposure at the site of action for small molecules, an ADC exposure–effect correlation is not known. Most ADC pharmacokinetic studies have focused on measuring systemic exposures of ADC species, but few investigations characterized the tissue catabolite that is ultimately responsible for efficacy and toxicity (5, 6). Recently, we reported that anti-CD22 linked PBD conjugates containing a cyclobutyl-substituted disulfide linker exhibited strong efficacy in a WSU-DLCL2 xenograft mouse model whereas an ADC derived from a closely-related cyclopropyl linker was inactive (7–9). The ADC exposures and drug-to-antibody ratios (DAR) between the two ADCs were similar in circulation. However, the former entity efficiently released its PBD payload in tumors while the latter only generated a non-immolating thiol-containing catabolite that did not effectively bind to DNA.

The learning from the qualitative assessment described above suggests that the PBD payload needs to be released in tumors at appropriate levels to result in cell killing. We, therefore, wanted to understand if there is a quantitative correlation between the efficacy exhibited by ADCs bearing PBD cytotoxic payload and corresponding intratumor payload exposures. Accordingly, the efficacy experiments in mouse xenograft models were conducted to employ the ADCs that contain methyl- and non-methyl

[1]Drug Metabolism & Pharmacokinetics, Genentech Inc., South San Francisco, California. [2]Translational Oncology, Genentech Inc., South San Francisco, California. [3]Discovery Chemistry, Genentech Inc., South San Francisco, California. [4]Protein Chemistry, Genentech Inc., South San Francisco, California. [5]Bioanalysis, Genentech Inc., South San Francisco, California.

Note: Supplementary data for this article are available at Molecular Cancer Therapeutics Online (http://mct.aacrjournals.org/).

Corresponding Author: Donglu Zhang, Genentech, Inc., South San Francisco, CA 94080. Phone: 650-291-0058; E-mail: zhang.donglu@gene.com

doi: 10.1158/1535-7163.MCT-17-0697

Published OnlineFirst January 18, 2018; DOI: 10.1158/1535-7163.MCT-17-0697

Table 1. The ADC structures, animal parameters, and systemic exposures in efficacy studies using ADCs containing PBD as payload in HER2-expressing MMTV-Fo5 xenograft models ($n = 8$ for efficacy analysis and $n = 3$ for exposure analysis)

ADC names		ADC structures[a]		Animal parameters	Systemic exposure		Efficacy (range, 95% CI)
Group	Description	Linker	Attaching site	Antigen	Tab[b] (μg/mL)	DAR at D10	AUC/day[c]
A1	HER2-HC-H-SS-PBD	H-Disulfide	HC A140C	HER2	20.7/0.67	0.9	88 (37, 146)
A2	HER2-LC-H-SS-PBD	H-Disulfide	LC K149C	HER2	24.1/5.04	1.0	63 (18, 120)
A3	HER2-HC-Me-SS-PBD	Me-Disulfide	HC A140C	HER2	1.41/0.35	1.7	44 (1, 89)
A4	HER2-LC-Me-SS-PBD	Me-Disulfide	LC K149C	HER2	1.42/0.02	1.6	114 (59, 190)

[a]ADCs had a DAR value of 1.9–2 with aggregation of <5% and free remaining linker payload of <2% that were prepared from THIOMAB antibody.
[b]Plasma data at Days 4 and 18 were shown following the dose of 4 mg/kg for A1/A2 and of 0.4 mg/kg for A3/A4. The payload PBD was not detected in plasma.
[c]The AUC/day values extrapolated from tumor size-time profile. TGI_{rel} was calculated from comparison of tumor growth in AUC/day of each treatment (for A1–A3) to that of the least-active entity A4 (Fig. 1A) as described in the Supplementary Data (17).

substituted disulfide linkers, have different conjugation sites as attachment sites may affect the conjugate stability (10), display a spectrum of plasma stabilities, and have a 10-fold dose gap to compensate the anticipated ADC immolation and stability difference (Table 1; Fig. 1). In addition to monitoring tumor growth, tumor and plasma samples were collected during these experiments at different time points from selected animals. The intratumor payload concentrations were determined along with total antibody (Tab) concentrations and DAR and these parameters were subsequently correlated with observed tumor sizes or growth. Furthermore, *in vitro* studies were conducted to understand the critical factors that determine payload concentrations in tumors.

Materials and Methods

Materials

Formic acid and calf thymus DNA were purchased from Sigma-Aldrich. Human HER2 and CD22 antibodies with two engineered cysteine residues (THIOMAB antibodies) were generated at Genentech as described previously (11–13). Mice (CB-17 SCID, female, nude, and Balb/C strains) were purchased from Charles Rivers Laboratories. All animal studies were carried out in compliance with the NIH guidelines for the care and use of laboratory animals and were approved by the Institutional Animal Care and Use Committee at Genentech, Inc. PBD, **LD1**, and **LD2** with a purity of >95% were synthesized as described previously (8, 14).

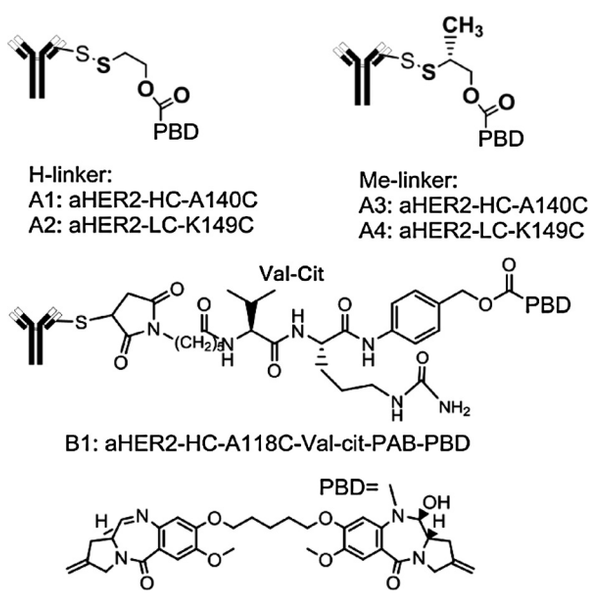

Figure 1.
Chemical structures of ADCs and catabolites (payloads) used in this study.

Preparation of ADC conjugates

Anti-HER2 conjugates on light chain K149C, heavy chain A140C of non-methyl- and methyl-disulfide linked PBD-dimer (A1: aHER2-HC-H-SS-PBD, A2: aHER2-LC-H-SS-PBD, A3: aHER2-HC-Me-SS-PBD, and A4: aHER2-LC-Me-SS-PBD) used in Groups A1–A4, and peptide-linked PBD ADC B1: aHER2-A118C-val-cit-PAB-PBD using group B1 were prepared as described previously (11–13). Briefly, full length, cysteine-engineered monoclonal antibodies (THIOMAB antibodies) were incubated with 50-fold of DTT overnight at room temperature to reduce disulfide bonds between the engineered cysteine residues and the cysteine or glutathione. Excess DTT was removed and buffer was exchanged using a 5-mL HiTrap SP cation exchange column attached to an Akta purification system (GE Healthcare) using a step-gradient of buffer B (50 mmol/L Tris, pH 8.0, 150 mmol/L NaCl) in buffer A (20 mmol/L succinate, pH 5.0) at a flow rate of 5 mL/min. The eluted reduced antibodies were treated with 15 equivalents of dehydroascorbic acid dissolved in N,N-dimethylacetamide for approximately 3 hours to allow the interchain disulfides to reform while leaving the engineered cysteines free for conjugation. Dehydroascorbic acid was removed on the same HiTrap SP column using a gradient of 30% to 100% buffer B (10 mmol/L succinate, pH 5.0, 300 mmol/L NaCl) in buffer A (10 mmol/L succinate, pH 5.0) over 30 column volumes at a flow rate of 5 mL/min and EDTA was added to the antibody stock. For conjugation, the antibody solutions were adjusted to pH 8.5 with 1 M Tris, pH 8.5. An excess of the nitropyridyl disulfides or maleimidocaproyl-valine-citrulline-p-animobenzyl linker drugs, dissolved in DMF, were added to the antibody solution. The conjugates were purified from the conjugation mixtures using disposable S maxi cation exchange columns (Pierce), binding and washing with 20 mmol/L histidine acetate, pH 5.5 and eluting at 5 mL/min in 20 mmol/L histidine acetate, pH 5.5, 300 mmol/L NaCl to remove the unconjugated linker drugs and conjugation byproducts. The final conjugates were formulated in a buffer of 20 mmol/L histidine-acetate, pH 5.5, 240 mmol/L sucrose containing 0.02% Tween-20. Analytical size exclusion chromatography (SEC) performed with a Shodex KW-802.5 column (8.0 × 300 mm, isocratic elution, 0.2 M potassium phosphate, pH 6.2, 0.25 mmol/L KCl, 15% isopropanol, flow rate = 0.75 mL/min) was used to measure aggregation. DAR was analyzed after digestion with the protease Lys-C (separating Fab and Fc domains on with reversed-phase LC/MS (PLRP-S column, 1000 Å,

Published OnlineFirst January 18, 2018; DOI: 10.1158/1535-7163.MCT-17-0697

50 mm × 2.1 mm; Polymer Laboratories) using a gradient of buffer B (0.05% TFA in acetonitrile) in buffer A (0.05% TFA in water) at 0.5 mL/min on an Agilent 1100 series time-of-flight (TOF) mass spectrometer (Agilent Technologies). Protein concentrations were determined using a BCA assay (Pierce). All conjugates had aggregation levels <5%, amounts of remaining unconjugated linker drug <2% at concentration of >2 mg/mL.

In vivo xenograft studies: efficacy and tissue collection

The Fo5 mouse mammary tumor model was employed to evaluate the *in vivo* efficacy of anti-HER2 disulfide linked PBD conjugates as described previously (15, 16). The Fo5 model is a transgenic mouse model in which the human HER2 gene is overexpressed in mammary epithelium under transcriptional regulation of the murine mammary tumor virus promoter (MMTV-HER2). The mammary tumor of one of these founder animals [founder 5 (Fo5)] has been propagated in subsequent generations of FVB mice by serial transplantation of tumor fragments (~2 mm × 2 mm in size). All treatment groups consisted of 8 animals per group. When tumor size reached a desired volume, animals were divided into groups of eight mice.

Mice were dosed IV via the tail vein with ADC conjugates A1–A4. A1 and A2 were dosed at 4 mg/kg and A3 and A4 were dosed at 0.4 mg/kg. Tumors and body weights of mice were measured one to two times a week throughout the study. Mice were promptly euthanized when body weight loss was >20% of their starting weight. All animals were euthanized before tumors reached 3000 mm^3 or showed signs of impending ulceration. Tumor volume was measured in two dimensions (length and width) using calipers and the tumor volume was calculated using the formula: Tumor size (mm^3) = (longer measurement × shorter measurement^2) × 0.5. The tumor volumes were plotted as a mean tumor volume of each group over time. Tumor stasis was defined as no tumor size change from day 0. Tumor growth inhibition (TGI) was calculated as percent area under the tumor size–time curve (AUC) per day of each treatment group in relation to vehicle or the least-active group A4 in MMTV-Fo5 xenograft models. The relative TGI (TGI_{rel}) was calculated as follows (16, 17):

$$\%TGI_{rel} = 100 \times (AUC_{treatment}/day/AUC_{vehicle\ or\ least\ active\ treatment}/day)$$

Accordingly, $\%TGI_{rel}$ in comparison to Group A4 were 22.8%, 44.7%, and 61.4% for Group A1, A2, and A3, respectively. The confidence intervals (CI) for %TGI were determined and the 2.5 and 97.5 percentiles of CIs were reported as the low and high range.

Plasma samples were collected from selected xenograft mice ($n = 3$) for each group for analysis of Tab concentration and DAR values. Plasma samples were collected at day 4, 10, and 18 for anti-HER2-PBD ADCs (A1–A4). Tumor tissues from satellite groups for each treatment groups were collected at day 4, 10, and 18. The vehicle control animals in the Fo5 xenograft study were terminated at Day 5 due to rapid tumor growth. The plasma and tissue samples were kept frozen at −80°C until being analyzed.

Dose-fractionation studies

Xenograft mice of MMTV-Her2/Fo5 ($n = 8$ each treatment group) were dosed with a single 1 mg/kg IV dose and 0.33 mg/kg doses every week three times with aHER2-A118C-val-cit-PAB-PBD ADC (ADC B1). Tumors and body weights of mice were measured one to two times a week throughout the 4-week study. Tumor volume was measured in two dimensions as described previously. The tumor volumes were plotted as a mean tumor volume SEM of each group over time.

Measurements of Tab and DAR

Tab concentration was determined by the ELISA method as described previously (18). Plasma samples from the stability study were analyzed for Tab (conjugated plus unconjugated antibody) concentrations in microtiter plates (384 wells; Nunc) that were coated with human HER2 (Genentech, Inc.). The limit of quantitation (LOQ) was 3 ng/mL.

The DAR value was determined as described previously (19). Briefly, an appropriate volume of mouse plasma was incubated at room temperature with the biotinylated HER2 target antigen, which was coupled to the streptavidin paramagnetic beads (Invitrogen). The bead captured ADC analytes were washed and deglycosylated at 37°C overnight. The resulting samples in 30% acetonitrile in water containing 1% formic acid were injected onto a Triple TOF 5600 mass spectrometer (AB Sciex) coupled with HPLC using a reversed-phase column. The compounds were eluted by a gradient of mobile phase A (water with 0.1 % formic acid) and mobile phase B (acetonitrile with 0.1% formic acid) at a flow rate of 5 μL/min. Positive time-of-flight (TOF) MS scan was acquired and processed. Peak deconvolution was performed to obtain the distribution profile of DAR0, DAR1, and DAR2 species, and the corresponding peak areas were measured. Subsequently, the relative ratio of each DAR and the average DAR value at each time point were calculated.

Characterization and quantitation of catabolites in tissues

To quantitate the concentrations of catabolites in the mouse plasma and tissues, the tumor samples were homogenized in control mouse plasma, and extracted by an acetonitrile to precipitate the proteins. The samples were injected to an AB Sciex Triple Quad 6500 mass spectrometer (MS) coupled with a Shimadzu liquid chromatography (LC). Peak separation was achieved and the matrix effects of the tissue samples were minimized by homogenizing the tissues in blank mouse plasma through identifying background peaks and using known amounts of PBD spiked into blank homogenized tissue as standards. It is noted that these ADCs may release more than one metabolite, some of which may not be active, and that only levels of active payload (PBD) were quantitated and compared in tissues.

DNA isolation and quantitation was performed as described previously (7). DNA extraction from mouse tumors: Mouse tumors were weighed and homogenized in four volumes of ice-cold PBS by weight. The plasma samples were diluted with four volumes of ice-cold PBS. DNA from 75 μL of homogenates or 15 μL plasma was isolated by DNeasy Blood & Tissue Kit following the instructions with the following modifications. After the first loading of tissue lysate, the flow-through was loaded two more times to ensure the best column binding of DNA. The columns were washed sequentially by two wash buffers containing 60% to 70% ethanol. In the last step, DNA on the column was eluted with 200 μL water twice and the eluates were combined.

DNA digestion and heating to release PBD: Aliquots of 200 μL DNA eluant were digested with 0.001 units of nuclease P1 at 37°C for 1 hour and then heated at 90°C for 30 minutes to release PBD. The post-heating samples were aliquoted for the separate quantitation of PBD and DNA. Stability of PBD in the absence of DNA was also tested under the same condition and PBD was found to be stable.

Published OnlineFirst January 18, 2018; DOI: 10.1158/1535-7163.MCT-17-0697

DNA and PBD quantitation: Isolated DNA was quantitated via measuring the deoxyadenosine monophosphate (dAMP) generated from nuclease P1 (NP1) digestion with calf thymus DNA as a standard by an LC/MS-MS method. Calf thymus DNA was dissolved in water at various concentrations and the linear range was 5 to 5,000 ng/mL for DNA quantitation. The DNA isolated from tissue samples was diluted 200-fold before quantitation. The digestion was complete as judged by the observation that no more dAMP was produced with additional NP1. The deoxyribonucleotides produced from DNA hydrolysis were analyzed on a Shimadzu Nexera HPLC system coupled to a Sciex API 6500 triple quadrupole mass spectrometer with an IonDrive Turbo V source (Sciex) in a positive ion mode. The column was Phenomenex XB-C18 100 × 2.1 mm, 2.6 μm with mobile phase A, water with 0.1% formic acid and mobile phase B, acetonitrile with 0.1% formic acid. The gradient was 0 to 1.0 minutes, 0% B, 1.0 to 2.0 minutes, 0% to 5% B, 2.0 to 2.5 minutes, 5% to 95 % B, 2.5 to 3.0 minutes, 95% B, 3.0 to 3.5 minutes, 95% to 0% B, 3.5 to 4.0 minutes, 0% B at a flow rate of 1.0 mL/min (column temperature, 50°C) with an injection volume of 10 μL. Inosine monophosphate (IMP at 50 ng/mL) in water was used as the internal standard. The retention times of dAMP, dTMP, dCMP, dGMP, and IMP were 1.41, 0.98, 0.54, 1.22, and 0.8 minutes, respectively. The PBD stock solutions were spiked into pure water or 100 μg/mL calf thymus DNA solution to make standard curve samples containing 0.2 to 7.8 nmol/L of PBD. The PBD samples were analyzed on AB Sciex triple quadrupole 6500 MS coupled with a Shimadzu LC. Peak separation was achieved using a Phenomenex Kinetex C18 column, 1.7 μm, 100 Å, 100 × 2.1 mm with mobile phase A (0.1% formic acid) and B (100% acetonitrile) using a gradient of 0 to 0.5 minutes 5% B, 0.5 to 3.5 minutes 5% to 90% B, 3.5 to 4.0 minutes 90% B, 4.0 to 4.5 minutes 90% to 5% B, 4.5 to 5.0 minutes 5% B at a flow rate of 0.5 mL/min (column temperature of 35°C). The retention times of PBD, and IS were 2.6, and 2.9 minutes, respectively. The multiple reaction monitor (MRM) transitions in MS was PBD (585.1/504.2) and IS (589.2/261.0).The LC/MS-MS analysis showed that the presence of DNA did not impact the recovery and quantitation of PBD since two standard curves in water and DNA solutions were nearly superimposed. Quantitative recovery of PBD from tissue DNA samples can be expected after the digestion and heating process.

Calculation of PBD-DNA adducts: The conversion of mass of nucleotides as determined by LC-MS/MS to molarity of DNA was based on the average molecular weight of a DNA base pair (of 650 Da). The final results were shown as the adduct numbers per million DNA base pairs. PBD-DNA adducts = PBD concentration/DNA concentration/650/10^9 × 10^6, for example. At day 4, PBD-DNA adducts = 0.65 (nmol/L)/[224(ng/L)/650 × 10^9] × 10^6 = 1.88 PBD/10^6 bp (7).

Calculation of ADC and catabolite exposures and plots with relative TGI

The Tab concentrations were determined and plotted against time (three time points for animals dosed with anti-HER2-PBD (Supplementary Fig. S1E). The area under the Tab-time curve (AUC) was estimated by a linear trapezoidal method (20). The average Tab-AUC values for each treatment group are plotted in Fig. 2B. The tumor concentrations were determined from tissues collected at day 4, 10, and 18 for DNA-bound PBD. These concentrations were plotted against TGI_{rel} (Fig. 2D). For DNA-bound PBD, the intratumor amount (/10^6 bp) and concentrations (nmol/L) were determined from tissue collected at day 4, 10, and 18. The area under the PBD amount or concentration–time curve (AUC) was also calculated by a linear trapezoidal method (20).

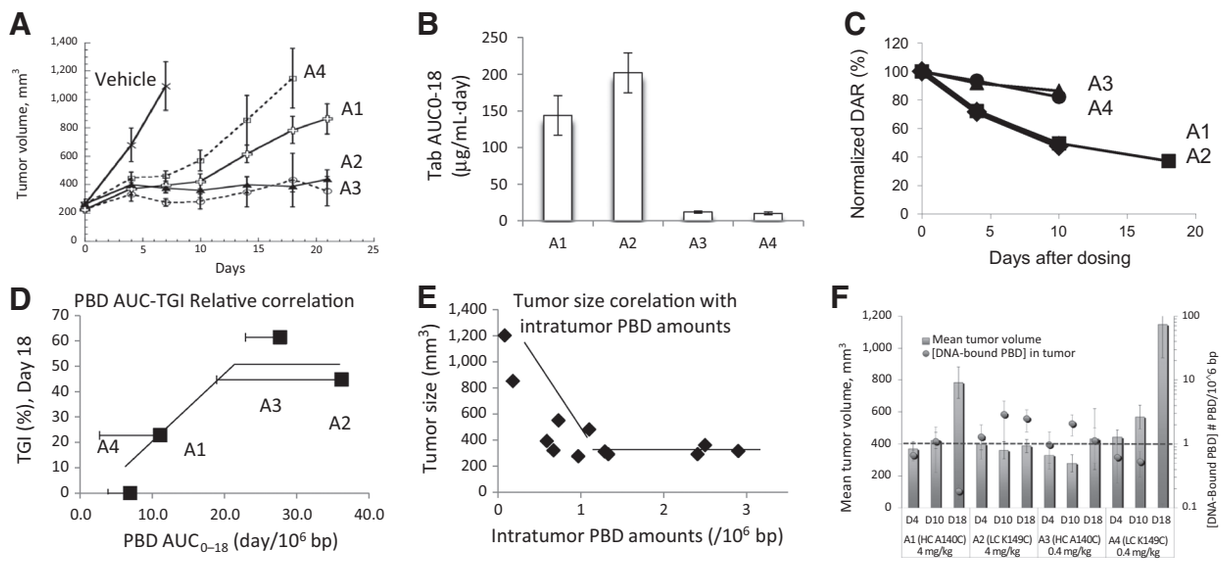

Figure 2.

A, *In vivo* efficacy of PBD-ADCs in mice bearing human HER2-expressing Fo5 xenografts (n = 8) after intravenous administration of corresponding ADCs A1–A4, A1 and A2 were dosed at 4 mg/kg whereas A3 and A4 were dosed at 0.4 mg/kg; **B,** Tab AUC values calculated from concentration data in Supplementary Table S2 of selected time points of 0–21 days; **C,** Normalized antibody-to-drug ratios and time profiles in plasma. The DAR for A1/A3/A4 at Day 18 was not measured due to a low concentration; **D,** Correlation X–Y plots of tumor sizes with corresponding intratumor DNA exposures (day/10^6 bp) at all time-points; **E,** Time- and dose-dependent correlation of tumor sizes with intratumor DNA-PBD adducts (/10^6 bp). The dot for A4 at Day 18 was not shown because the tumor concentration had a value 0.08/10^6 bp that is lower than the minimal Y axis mark of 0.1.

Published OnlineFirst January 18, 2018; DOI: 10.1158/1535-7163.MCT-17-0697

These intratumor PBD exposures were plotted against the TGI_{rel} (Fig. 2D; Supplementary Fig. S1D) and the trend lines were drawn in these X–Y plots.

Product identification from disulfide cleavage and linker immolation of nitropyridyl disulfide linker drugs LD1-2 and ADCs A1–A4

The nitropyridyl disulfide linker drug LD1 and LD2 at 5 μmol/L and ADC A1, A2, A3, or A4 at 0.3 mg/mL, 2 μmol/L) were incubated with 0.2 mmol/L cysteine in 100 mmol/L citric acid buffer (pH 5.5) or 100 mmol/L Tris buffer (pH 7.0) containing 5% methanol at 37°C. Aliquots were taken at 0, 1, 4 (or 5), and 24 hours and the samples were analyzed by LC/MS on Sciex Triple-TOF 5600 on a Hypersil Gold C18 column (100 × 2.1, 1.9 μmol/L; Thermo Scientific). The column was eluted by a gradient of buffer A (0.1% formic acid in 10 mmol/L ammonium acetate) to buffer B (0.1% formic acid in 10 mmol/L ammonium acetate in 90% acetonitrile), 5% B 0 to 0.5 minutes, 5% to 25% B 0.5 to 8 minutes, 25% to 75% B 8–13 minutes, and 75% to 95% B 13 to 13.5 minutes, 95% B 13.5 to 14.5 minutes, 95% to 5% B 14.5 to 15 minutes at 0.4 mL/min. All products were separated and characterized by LC/MS-MS in a positive ESI ion mode. All analytes had the protonated molecular MH+ as the major species with little source fragmentation. Full scan accurate mass peak areas were used to estimate relative abundance of each species.

Thiol 1a and Thiol 1b had the same molecular ions and fragmentation patterns but different retention times. These two products were proposed to be the stereoisomers that resulted from intramolecular cyclization of the thiol intermediates following disulfide linker cleavage. For the same reason, Thiol 2a and Thiol 2b are the stereoisomers from the methyl-disulfide linkers. The cyclization reactions of these thiol intermediates are reversible, which eventually will immolate to lead to formation of payload PBD.

Results

Table 1 lists the ADC structures, animal model parameters, systemic ADC exposures, and efficacy for ADCs A1–A4. Figure 1 lists the chemical structures of ADC molecules and catabolites used in this study. Multiple parameters were examined for correlation with the observed efficacy in xenograft models. Importantly, Fig. 2 and Supplementary Fig. S1 show that TGI_{rel} (efficacy) profiles (17) correlate well with intratumor payload concentrations/AUC or amounts but not with ADC systemic exposures (Tab AUC) following intravenous administration.

Figure 2D–F and Supplementary Fig. S1A–S1D show that there is a good trend correlation between antitumor activity and intratumor PBD exposures (AUC estimates from sparse sampling and may not be statistically significant due to the individual variability) or PBD amounts at individual time points (Day 4, 10, or 18) in HER2-expressing MMTV-Fo5 xenograft models following single doses of ADCs A1–A4. These four ADCs incorporate two types of disulfide linkers (non-methyl disulfide and methyl disulfide), and two attachment sites (LC K149C and HC A140C) and two doses (4 and 0.4 mg/kg) were employed in the described experiments (Fig. 1). Our previous study established that the number of PBD molecules per 10^6 base pair that was covalently bound to DNA at the site of action can be determined, and the majority of PBD delivered intracellularly via an ADC preferentially forms DNA adducts as opposed to remaining in the cytoplasm (7). Accordingly, the subcellular amount of PBD was determined and correlated with TGI_{rel} values of ADC conjugates A1, A2, A3 relative to the day 0 to 18 tumor growth curve of ADC A4. In this analysis, the vehicle control animals in the Fo5 xenograft study were terminated at Day 5 due to rapid tumor growth and could thus not be utilized for standard TGI calculations (16, 17). Instead, relative comparisons (TGI_{rel}) of 0- to 21-day TGI were made among the different conjugates with that of the least-active entity (ADC A4). As apparent in Fig. 2D, intratumor PBD exposures correlated with antitumor activity showing the intratumor PBD $AUC_{0\text{-}18}$ values (AUC during 0–18 days) in excess of 20 day/10^6 bp affording a maximum level of efficacy ("Plateau"). The correlation appears to be similar when the AUC (0–18 days) of PBD that covalently bound to DNA (Fig. 2D), AUC of intratumor PBD concentrations (Supplementary Fig. S2D), or PBD amounts in Day 4, 10, or 18 tumors (Supplementary Fig. S1A–S1C) were used. In addition, when tumor sizes (Y-axis) from all groups at all-time points were plotted against the PBD amount (*x*-axis) in the corresponding groups (Fig. 2E), the PBD amount needs to be approximately $1/10^6$ PBD/bp to achieve tumor stasis. Furthermore, when the tumor size was plotted against the amount of intratumor PBD at the corresponding time, there also appears to be a threshold PBD amount needed to cause TGI (Fig. 2F). Interestingly, payload amounts in tumor increased for all four conjugates from Day 4 to Day 10, but for only ADCs A2 and A3, the amounts of the PBD payload reached an initial threshold (C_{tumor}) to support the tumor stasis/regression and the value was not significantly diminished over 3 weeks after single doses (Supplementary Table S1). In comparison, an initial threshold of payload amount was not reached for tumor stasis for ADCs A1 and A4, which led to continuing growth of tumors and eventually much dilution of PBD payload in tumors at Day 18 (0.18, and 0.08 for ADCs A1 and A4 vs. 2.50, and $1.14/10^6$ bp for ADCs A2 and A3, respectively).

Another important observation from the assembled data is that the intratumor payload concentrations may reach a threshold beyond which additional efficacy is not achieved. For example, ADC conjugates A2 and A3 afforded similar efficacies in the Fo5 model (Fig. 2A), but the former entity delivered greater amounts of the PBD payload to the targeted tumors (Fig. 2D; Supplementary Table S1A). If the ADC was to be dosed every three weeks, this extra payload delivery did not improve the antitumor efficacy, but would generate more payload in normal tissues that may lead to toxicity although there was no apparent body weight loss from these xenograft mice (Supplementary Fig. S1F).

Attachment sites and linker types appeared to affect the ADC stability, systemic exposures, and the efficacy (Fig. 2B and C; Supplementary Fig. S1E). ADC A2 (non-methyl linker ADC at LC K149C) and ADC A3 (methyl-linker at HC A140C) appeared to achieve similar efficacy of tumor stasis (Fig. 2A), however, the doses and associated Tab exposures (AUCs) for these ADCs had difference by 10-fold with DAR loss (instability) for ADC A2 (Fig. 2B and C; Supplementary Table S1B). Similarly, ADC A1 (non-methyl linker ADC at HC A140C) and ADC A4 (methyl-linker at LC K149C) appeared to achieve partial TGI (Fig. 2A). However, the doses and associated Tab exposures (AUCs) for these ADCs had 10-fold difference with DAR loss (instability) for ADC A4 (Fig. 2A–C; Supplementary Table S1B). For the non-methyl linker ADCs, LC K149C attachment (A2) was more efficacious than HC A140C attachment (A1) at the same 4 mg/kg dose and the efficacy

Published OnlineFirst January 18, 2018; DOI: 10.1158/1535-7163.MCT-17-0697

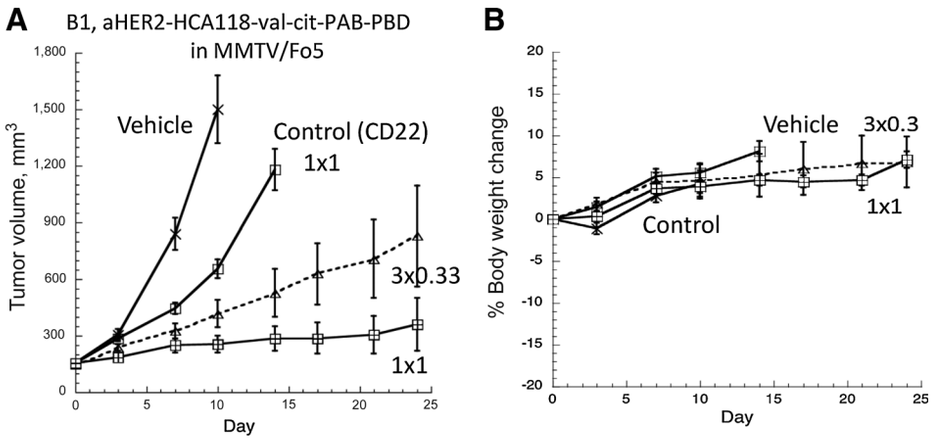

Figure 3.

A, Dose-fractionation efficacy studies of PBD-containing ADC B1 in xenograft mice bearing human HER2-expressing Fo5. Xenograft mice ($n = 8$ each treatment group) were dosed with a single IV dose or one third of the dose very week three times. Tumors in mice were measured one to two times a week throughout the studies. The tumor volumes were plotted as a mean tumor volume SEM of each group over time. **B,** Body weights from the *in vivo* efficacy study in mice bearing human HER2-expressing Fo5.

order apparently switched for the methyl-linker ADCs with the two attachment sites (A3 for HC A140C versus A4 for LC K149C) at the 0.4 mg/kg dose. Despite all above inconsistency, the efficacy for LC K149C versus HC A140C attachment with the non-methyl- and methyl-linkers was consistent with corresponding intratumor payload concentrations. The site of attachment and linker stability apparently impacted ADC plasma stability and exposures that in turn afforded the very different intratumor payload levels observed, especially at a later time point (Supplementary Table S1A).

These results indicated that the antitumor efficacy showed correlation with the intratumor PBD exposures with a `plateau' effect. There does not appear to be any consistent correlation of the efficacy with other parameters such as Tab exposures, extrapolated conjugated antibody exposures (Tab multiplied by DAR), dose, linker, attachment site, and plasma stability (DAR changes). These results also suggest that short-term payload assessments in tumors could be utilized to predict the efficacy of ADCs in preclinical efficacy experiments.

Dose-fractionation studies

The above correlation results of TGI with intratumor payload exposures suggest that the intratumor payload concentration (C_{tumor}) drives the ADC efficacy. To test whether there is a threshold payload concentration needed for efficacy, we performed dose-fractionation studies to compare to the efficacy results from a single dose and fractionated doses. In Fig. 3A, a single 1 mg/kg dose of an anti-HER2-val-cit-PAB PBD ADC (ADC B1) shows tumor stasis in the MMTV-Her2/Fo5 model for over 3 weeks, but when this dose was administered each week three times at 0.33 mg/kg, only partial TGI was achieved. Although the total dose and total systemic antibody exposures from 1 mg/kg and 3 × 0.33 mg/kg were similar, the single dose showed a much better efficacy and body weights showed slight increases in all groups (Fig. 3B). A smaller initial dose could not supply a sufficient concentration of payload to cause TGI and additional doses did not further improve the partial efficacy (did not break the trend of tumor growth). Consistent with our intratumor PBD analysis results in last study, once a threshold intratumor PBD concentration (C_{tumor}) is reached to achieve an antitumor activity (tumor stasis) from an initial 1 mg/kg dose, no additional doses were needed to sustain the tumor stasis or tumor reduction as a minimal efficacious dose. A much lower level of efficacy was observed with the nontarget ADC (anti-CD22-control, 3 mg/kg) in these experiments.

Mechanistic studies: immolation and disulfide stability

Payload release would require immolation following disulfide linker cleavage. For easy product detection, we studied linker immolation by incubating the nitropyridyl linker drugs (LD1 and LD2) at a higher concentration (5 μmol/L). As shown in Fig. 4A and B, the disulfide bond was quickly cleaved within 1 hour in the presence of cysteine. Although the methyl-linker drug LD2 generated the immolated product PBD (Fig. 4A), most of the resulting products from non-methyl linker LD1 were the thiol intermediates (Thiol 1a and Thiol 1b) at 1 and 4 hours (Fig. 4B). These results suggested that methyl-containing linker immolates much more efficiently than the non-methyl-containing linker. The structures of the intermediates Thiol 1a and Thiol 1b are consistent with the stereoisomer of intramolecular cyclization (Fig. 4C). The corresponding thiol intermediates (Thiol 2a and Thiol 2b) were minor products from the methyl-containing LD2 because of efficient linker immolation (Fig. 4A).

The stability of the disulfide bond in the ADC conjugates was tested in the *in vitro* incubation of an ADC in the presence of cysteine. The respective major product of non-methyl-linker ADCs A1/A2 and methyl-linker ADCs A3/A4 was the expected thiol intermediates and PBD, which were used to assess the stability of the corresponding disulfide bond. PBD was the major product of methyl-linker ADCs (A3 and A4) under both lysosomal condition (pH 5.5) and a neutral condition (pH 7.0) and of non-methyl linker ADCs (A1 and A2) under a neutral condition (pH 7.0). Formation of Thiol 1a/1b and PBD increased with time from 1 to 24 hours for all conjugates (Fig. 5A and B). The lower levels of formation of Thiol 1a/1b (A1 < A2) and PBD (A3 < A4) from the A140C connection in A1 and A3 than the K149C connection in A2 and A4 support that A140C conjugation protects the disulfide bond from cysteine accessibility for reduction. The higher stability of the methyl-substituted disulfide bonds limited the disulfide cleavage and subsequent PBD release although the immolation was faster, which led to lower levels of PBD formation (A3/A4 < A1/A2, in Fig. 5C and D; Supplementary Fig. S2). Therefore, payload release is a net result of disulfide cleavage and subsequent immolation. *In vitro*, the disulfide stability is a more important factor than immolation for payload release.

Discussion

Many disease target-related, ADC structure-related, and patients (xenograft models)-related variables could impact ADC

Published OnlineFirst January 18, 2018; DOI: 10.1158/1535-7163.MCT-17-0697

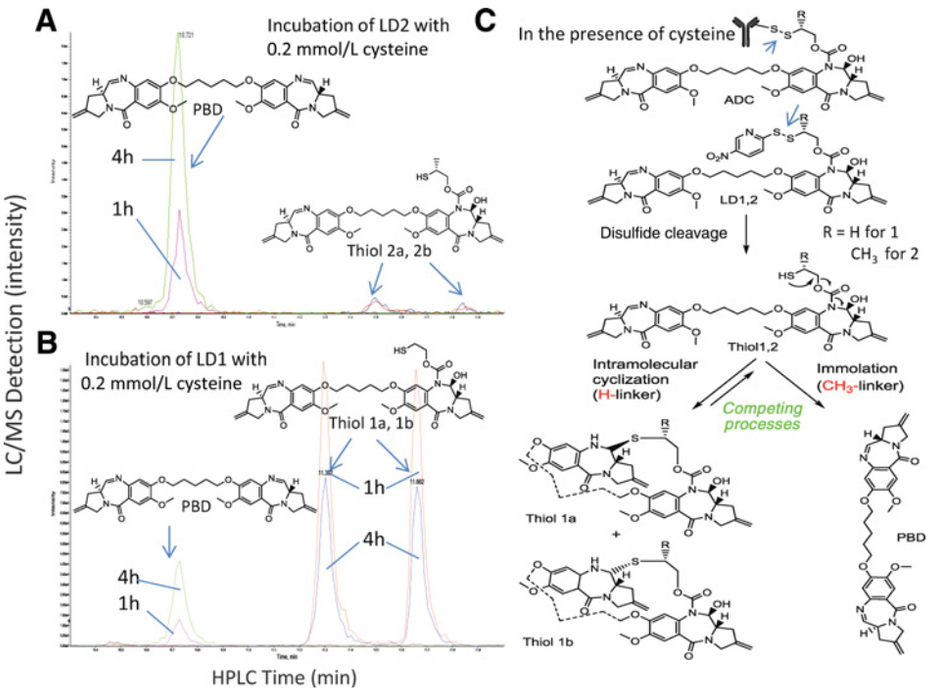

Figure 4.
Catabolite identification and payload release mechanism of H- (non-methyl) and Me- (methyl) disulfide linkers from nitropyridyl disulfide PBD linker drugs (LD1 and LD2) in the presence of cysteine at pH 5.5.

efficacy and toxicity. A threshold concentration of payload over time in target tissues would be required to trigger and support efficacy. In this study, the payload concentration C_{tumor} was widely separated at Day 18 even at Day 10, although C_{tumor} at Day 4 seemed to be similar between these four ADCs (A1, A2, A3, and A4), which supports that a threshold PBD concentration (C_{tumor}) was achieved for ADCs A2 and A3 to sustain the corresponding TGI. In the cases described here, intratumor PBD AUC values or amounts at Day 4, 10, and 18 correlated with Day 0 to 21 TGI in a HER2-tumor model. Use of total payload concentrations instead of free fraction in tumors for correlation is logical because PBD covalently bound to target DNA. In these correlation

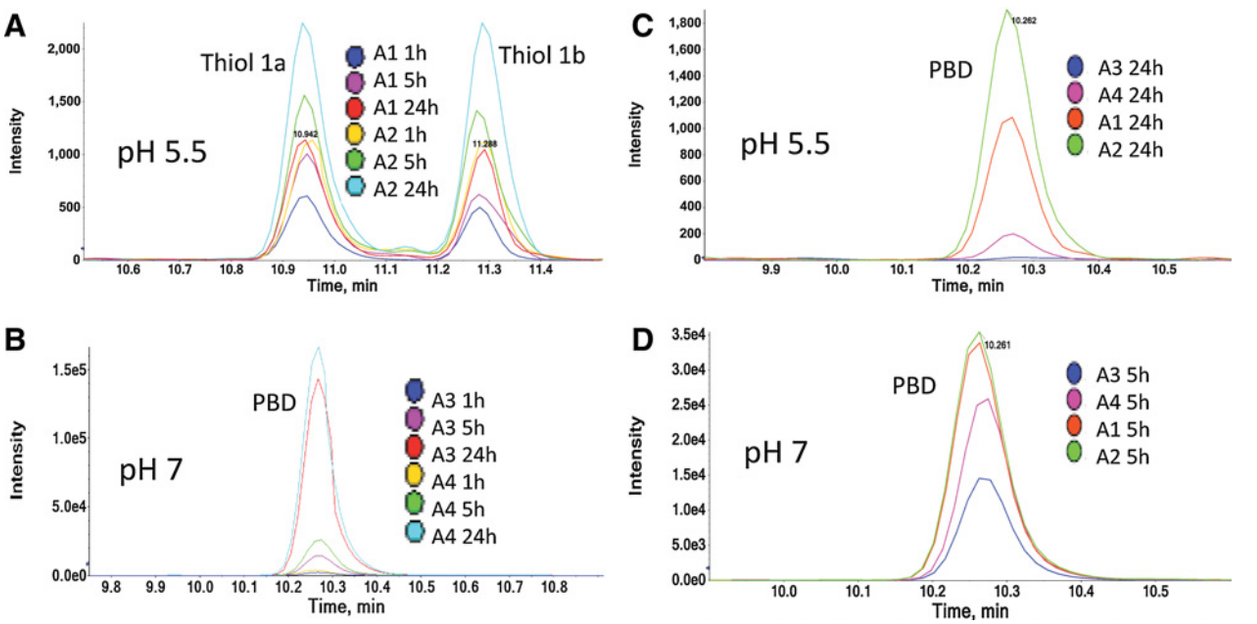

Figure 5.
Disulfide stability assessed by formation of major catabolites and payload release of ADC A1–A4 in the presence of cysteine at pH 5.5 or 7.0. Data from other time points are presented in Supplementary Fig. S2.

Published OnlineFirst January 18, 2018; DOI: 10.1158/1535-7163.MCT-17-0697

relationships as expressed by X–Y plots (Fig. 2D–F; Supplementary Fig. S1A–S1D), there appeared to be (i) an apparent range of improving efficacy with increasing catabolite amounts or concentrations followed by a plateau, (ii) a threshold payload concentration that is required to support tumor stasis. This threshold concentration was approximately 1 PBD/10^6 bp for PBD-ADC, and (iii) a region of oversupply of payload in which increased payload concentration stopped improving tumor growth regression ("plateau" effect or E_{max}) but may contribute to toxicity. These correlations suggest that the assessment of the intratumor catabolite amounts or concentrations to support a maximal efficacy should be achievable, which was demonstrated with subsequent dose-fractionation study. Recognition of payload concentrations for efficacy "plateau" is important as the extra payload delivery to tumors do not improve efficacy but at a dose or systemic ADC exposure that will generate a higher catabolite concentration in normal tissues to cause toxicity.

There did not appear to be any consistent correlation between the efficacy and systemic exposures of ADCs along with linker, site of payload attachment, and plasma stability. It required a 10-fold dose and more than 15-fold higher plasma exposure for ADC A2 than ADC A3 to achieve a similar efficacy of tumor stasis. Although the Tab concentration was much higher for ADC A1/A2 than ADC A3/A4, approximately 66% to 75% of ADC was cleared from Day 4 to Day 10 for all these ADCs. These results suggested that target-mediated clearance was saturated for all ADCs at both 0.4 and 4 mg/kg doses. The much lower level of efficacy of ADC A1 with a 4 mg/kg dose than ADC A3 with a 0.4 mg/kg dose suggested that the target saturation did not play a role in determining their efficacy that was only determined by their corresponding tumor payload exposures. Although an ADC helps deliver the payload to tissues, the payload is ultimately responsible for efficacy and toxicity. Therefore, lack of correlation between the systemic exposure and efficacy is not surprising but does not suggest that the measurement of ADC plasma stability and systemic exposures is unimportant. Consistent with the results presented here, the ADCs with unstable sites of attachment leading to fast clearance and low efficacy might actually never deliver a threshold concentration of payload to tumors to achieve efficacy (21). In addition, increased doses of a given ADC in preclinical models or patients should lead to increased ADC systemic exposures and deliver more catabolite to tumors; however, a quantitative correlation between systemic exposure and ADC efficacy is not known (22, 23).

In vitro investigation revealed that both linker immolation and disulfide bond stability were the critical factors that would determine payload drug concentrations in tumors. The data in Fig. 4 suggested that the non-methyl disulfide linker used in ADC A1/A2 led to formation of relatively stable non-immolation products (Thiol 1a/1b) while the methyl-disulfide linker used in ADC A3/A4 immolated quickly to release PBD following the disulfide cleavage. In addition, the *in vitro* disulfide stability seems to be consistent with plasma stability with less DAR loss in xenograft mice for the methyl-substituted linker ADCs A3/A4 compared to those in non-methyl-substituted linker ADCs A1/A2 (Figs. 2C and 5; Supplementary Fig. S2). Data extrapolation from *in vitro* to *in vivo* suggest that lower disulfide instability that was associated with plasma instability plus slow immolation for the non-substituted disulfide linker led to the need of much higher doses for ADCs A1 and A2 to achieve similar levels of intratumor payload and TGI than ADCs A3 and A4. For the methyl-linker ADCs A3 and A4 without limitation of immolation, the availability of the ADC molecule to tumors is a key factor that determines the payload drug concentration in tissues; consequently, low dose plus relative instability of ADC A4 led to a lower level of efficacy than ADC A3. For non-methyl linker ADCs A1 and A2, immolation/payload releasibility is a key factor that determines the payload concentration in tissues; consequently, slow immolation plus disulfide cleavage that is subject to immolation led to less payload drug in tumors from ADC A1 than A2 with corresponding lower level of efficacy. Therefore, both immolation and supply of the ADC molecule to tumor that was determined by disulfide substitution-related plasma instability play important roles in determining payload drug concentrations and corresponding efficacy. These studies provide solid examples of (i) proper payload release is required for cell killing activity, (ii) *in vitro* disulfide stability is consistent with ADC *in vivo* stability that determines ADC supply to tumors, which augments linker cleavage in the tissue, and (iii) immolation and ADC stability together determine payload drug concentrations in tumor.

Although circulating catabolite rarely contributed to ADC efficacy due to the low concentration, a catabolite in circulation could contribute to ADC toxicity. Therefore, an instable ADC may show a low systemic exposure with less amount of catabolite delivered to tumors to give a low efficacy. However, the instability may generate a higher level of catabolite into circulation leading to toxicity. Despite having comparable efficacy, ADCs with maytansinoids linked through instable disulfide linker to anti-HER2 (with lower ADC exposure) showed greater weight loss in rats than a trastuzumab ADC linked through stable non-cleavable ether (15). Another example of exposure-response disconnect is that a 25%-exposure increase through incorporation of more stable bromoacetamidecaproyl linker of MMAE-ADC did not result in significant efficacy improvement compared to the reference ADC using maleimidocaproyl linker (24). Case studies described in this report have demonstrated that intratumor payload exposures correlate with efficacy, which requires that a threshold concentration of payload (C_{tumor}) is achieved in an initial period after dosing to exert a desired pharmacological activity relative to the 7-week efficacy of tumor stasis observed with an analog PBD ADC (9). The threshold payload PBD concentration must have been crossed in the previous study that showed tumor regression with single and multiple dose Anti-CD70-PBD ADCs in a xenograft model although the intratumor payload concentrations were not measured (25). An important factor to achieve the threshold payload concentration (as a PBD/DNA ratio) would depend on the ADC-mediated DNA alkylation accumulation rate versus the reversal of accumulation due to DNA repair. This factor is likely to be highly variable across xenografts depending on tumor properties such tumor type, size, and antigen expression levels as well as ADC properties such as internalization and catabolism.

In summary, intratumor catabolites correlate with ADC efficacy and that the efficacy is saturable (i.e., plateaus) after a threshold intratumor payload concentration is reached. These new concepts provided insights for ADC efficacy in two important aspects. First, ADC optimization should not rely on traditional pharmacokinetic studies of systemic exposures of ADC species. This approach is widely used for small molecule drug discovery, but a correlation between ADC plasma concentrations and efficacy is not known. Second, a threshold concentration of intratumor catabolites that is properly released is required to support sustained efficacy.

Importantly, an ADC can deliver an excessive level of payload to tumors beyond this threshold efficacy ("Plateau" effect) was not enhanced at a dose that may cause increased toxicity in normal tissues. The fractionation dosing experiments demonstrate a practical approach to discover the minimally efficacious dose level for a given ADC. With establishment of the correlation between intratumor catabolite exposures and antitumor efficacy, it will be valuable to predict intratumor catabolite exposures from the systemic exposure of ADC species.

Disclosure of Potential Conflicts of Interest

No potential conflicts of interest were disclosed.

Authors' Contributions

Conception and design: D. Zhang, S.-F. Yu, S.C. Khojasteh, J.D. Sadowsky, A.G. Polson, P.S. Dragovich, C. E.C.A. Hop
Development of methodology: D. Zhang, Y. Ma, K. Xu
Acquisition of data (provided animals, acquired and managed patients, provided facilities, etc.): S.-F. Yu, Y. Ma, J.D. Sadowsky, K. Xu
Analysis and interpretation of data (e.g., statistical analysis, biostatistics, computational analysis): D. Zhang, S.-F. Yu, Y. Ma, D. Su, K. Xu, C. E.C.A. Hop
Writing, review, and/or revision of the manuscript: D. Zhang, Y. Ma, T.H. Pillow, D. Su, K.R. Kozak, K. Xu, P.S. Dragovich, C. E.C.A. Hop
Administrative, technical, or material support (i.e., reporting or organizing data, constructing databases): S.-F. Yu, T.H. Pillow
Study supervision: D. Zhang, S.-F. Yu, K. Xu

Acknowledgments

We would like to thank Saileta Prabhu, Geoffrey Del Rosario, Jintang He, Corinna Lei, Luna Liu, and Isabel Figueroa Amenabar, Paul Polakis, Hans Erickson for their technical contributions.

The costs of publication of this article were defrayed in part by the payment of page charges. This article must therefore be hereby marked *advertisement* in accordance with 18 U.S.C. Section 1734 solely to indicate this fact.

Received July 21, 2017; revised September 14, 2017; accepted December 8, 2017; published OnlineFirst January 18, 2018.

References

1. Doronina SO, Toki BE, Torgov MY, Mendelsohn BA, Cerveny CG, Chace DF, et al. Development of potent monoclonal antibody auristatin conjugates for cancer therapy. Nat Biotechnol 2003;21:778–84.
2. LoRusso PM, Weiss D, Guardino E, Girish S, Sliwkowski MX. Trastuzumab emtansine: a unique antibody-drug conjugate in development for human epidermal growth factor receptor 2-positive cancer. Clin Cancer Res 2011; 17:6437–47.
3. Antonow D, Thurston DE. Synthesis of DNA-interactive pyrrolo[2,1-c][1,4]benzodiazepines (PBDs). Chem Rev 2011;111:2815–64.
4. Jeffrey SC, Burke PJ, Lyon RP, Meyer DW, Sussman D, Anderson M, et al. A potent anti-CD70 antibody-drug conjugate combining a dimeric pyrrolobenzodiazepine drug with site-specific conjugation technology. Bioconjug Chem 2013;24:1256–63.
5. Alley SC, Zhang X, Okeley NM, Anderson M, Law CL, Senter PD, et al. The pharmacologic basis for antibody-auristatin conjugate activity. J Pharmacol Exp Ther 2009;330:932–8.
6. Erickson HK, Lewis Phillips GD, Leipold DD, Provenzano CA, Mai E, Johnson HA, et al. The effect of different linkers on target cell catabolism and pharmacokinetics/pharmacodynamics of trastuzumab maytansinoid conjugates. Mol Cancer Ther 2012;11:1133–42.
7. Ma Y, Khojasteh SC, Hop CE, Erickson HK, Polson A, Pillow TH, et al. Antibody drug conjugates differentiate uptake and DNA alkylation of pyrrolobenzodiazepines in tumors from organs of xenograft mice. Drug Metab Dispos 2016;44:1958–62.
8. Zhang D, Pillow TH, Ma Y, Cruz-Chuh JD, Kozak KR, Sadowsky JD, et al. Linker immolation determines cell killing activity of disulfide-linked pyrrolobenzodiazepine antibody-drug conjugates. ACS Med Chem Lett 2016;7:988–93.
9. Zhang D, Yu SF, Ma Y, Xu K, Dragovich PS, Pillow TH, et al. Chemical structure and concentration of intratumor catabolites determine efficacy of antibody drug conjugates. Drug Metab Dispos 2016;44:1517–23.
10. Vollmar BS, Wei B, Ohri R, Zhou J, He J, Yu SF, et al. Attachment site cysteine Thiol pKa is a key driver for site-dependent stability of THIOMAB antibody-drug conjugates. Bioconjug Chem 2017.
11. Bhakta S, Raab H, Junutula JR. Engineering THIOMABs for site-specific conjugation of thiol-reactive linkers. Methods Mol Biol 2013;1045:189–203.
12. Junutula JR, Gerber HP. Next-generation antibody-drug conjugates (ADCs) for cancer therapy. ACS Med Chem Lett 2016;7:972–3.
13. Polson AG, Williams M, Gray AM, Fuji RN, Poon KA, McBride J, et al. Anti-CD22-MCC-DM1: an antibody-drug conjugate with a stable linker for the treatment of non-Hodgkin's lymphoma. Leukemia 2010;24:1566–73.
14. Pillow TH, Schutten M, Yu SF, Ohri R, Sadowsky J, Poon KA, et al. Modulating therapeutic activity and toxicity of pyrrolobenzodiazepine antibody-drug conjugates with self-immolative disulfide linkers. Mol Cancer Ther 2017;16:871–8.
15. Lewis Phillips GD, Li G, Dugger DL, Crocker LM, Parsons KL, Mai E, et al. Targeting HER2-positive breast cancer with trastuzumab-DM1, an antibody-cytotoxic drug conjugate. Cancer Res 2008;68:9280–90.
16. Pillow TH, Tien J, Parsons-Reponte KL, Bhakta S, Li H, Staben LR, et al. Site-specific trastuzumab maytansinoid antibody-drug conjugates with improved therapeutic activity through linker and antibody engineering. J Med Chem 2014;57:7890–9.
17. Yu SF, Zheng B, Go M, Lau J, Spencer S, Raab H, et al. A novel anti-CD22 anthracycline-based antibody-drug conjugate (ADC) that overcomes resistance to auristatin-based ADCs. Clin Cancer Res 2015;21:3298–306.
18. Kozak KR, Tsai SP, Fourie-O'Donohue A, dela Cruz Chuh J, Roth L, Cook R, et al. Total antibody quantification for MMAE-conjugated antibody-drug conjugates: impact of assay format and reagents. Bioconjug Chem 2013; 24:772–9.
19. Xu K, Liu L, Saad OM, Baudys J, Williams L, Leipold D, et al. Characterization of intact antibody-drug conjugates from plasma/serum *in vivo* by affinity capture capillary liquid chromatography-mass spectrometry. Anal Biochem 2011;412:56–66.
20. Perrier D, Gibaldi M. General derivation of the equation for time to reach a certain fraction of steady state. J Pharm Sci 1982;71:474–5.
21. Shen BQ, Xu K, Liu L, Raab H, Bhakta S, Kenrick M, et al. Conjugation site modulates the *in vivo* stability and therapeutic activity of antibody-drug conjugates. Nat Biotechnol 2012;30:184–9.
22. Kamath AV, Iyer S. Preclinical pharmacokinetic considerations for the development of antibody drug conjugates. Pharm Res 2015;32: 3470–9.
23. Lin K, Rubinfeld B, Zhang C, Firestein R, Harstad E, Roth L, et al. Preclinical development of an anti-NaPi2b (SLC34A2) antibody-drug conjugate as a therapeutic for non-small cell lung and ovarian cancers. Clin Cancer Res 2015;21:5139–50.
24. Alley SC, Benjamin DR, Jeffrey SC, Okeley NM, Meyer DL, Sanderson RJ, et al. Contribution of linker stability to the activities of anticancer immunoconjugates. Bioconjug Chem 2008;19:759–65.
25. Jeffrey SC, Torgov MY, Andreyka JB, Boddington L, Cerveny CG, Denny WA, et al. Design, synthesis, and *in vitro* evaluation of dipeptide-based antibody minor groove binder conjugates. J Med Chem 2005;48: 1344–58.

Published OnlineFirst January 18, 2018; DOI: 10.1158/1535-7163.MCT-17-0697

Molecular Cancer Therapeutics

Intratumoral Payload Concentration Correlates with the Activity of Antibody–Drug Conjugates

Donglu Zhang, Shang-Fan Yu, S. Cyrus Khojasteh, et al.

Mol Cancer Ther 2018;17:677-685. Published OnlineFirst January 18, 2018.